PCCP

New structural model of a chiral cubic liquid crystalline phase

Journal:	*Physical Chemistry Chemical Physics*
Manuscript ID	CP-ART-03-2020-001579.R1
Article Type:	Paper
Date Submitted by the Author:	04-May-2020

Complete List of Authors:	Vaupotič, Nataša; University of Maribor, Faculty of Natural Sciences and Mathematics; Institut Jozef Stefan, Salamończyk, Mirosław; University of Warsaw, Faculty of Chemistry; E O Lawrence Berkeley National Laboratory, Advanced Light Source Matraszek, Joanna; University of Warsaw, Faculty of Chemistry Vogrin, Martin; University of Hamburg, Department of Mathematics Pociecha, Damian; University of Warsaw, Faculty of Chemistry Gorecka, Ewa; University of Warsaw, Faculty of Chemistry

ARTICLE

New structural model of a chiral cubic liquid crystalline phase

Nataša Vaupotič,[a,b,*] Mirosław Salamończyk,[c,d] Joanna Matraszek,[c] Martin Vogrin,[e] Damian Pociecha,[c] Ewa Gorecka[c,*]

Received 00th January 20xx,
Accepted 00th January 20xx

DOI: 10.1039/x0xx00000x

We have studied properties of novel thermotropic mesogenic materials that exhibit both an achiral double gyroid ($Ia\bar{3}d$ symmetry) and chiral cubic phase (previously assigned the $Im\bar{3}m$ symmetry). We argue that in the chiral cubic phase molecules form micelles and channels arranged into continuously interconnected hexagons. From the x-ray diffraction experiment supported by modelling, exact positions of hexagons and their connections were deduced and showed to be embedded on a WP (degenerated Neovius) minimal primitive surface. The elastic energy of such a structure is close to the one of the double gyroid phase, which is in agreement with a very low enthalpy change observed at the phase transition. We also argue that the chirality of the phase is related to the lack of mirror symmetry of non-flat hexagons accompanied by an alternating inclination of molecules in the neighbouring segments of hexagon; the chirality of individual hexagon is amplified on the whole hexagon network by steric effects.

In soft matter, phases that contain three dimensional (3D) organization of channels have attracted a lot of interest, both due to their complexity as well as potential applications, for example as mechanically resistant materials [1], in photovoltaic [2], photonic devices and as optical metamaterials [3]. To date, most of the studies related to the continuous phases have been carried out for polymers and lyotropic systems, in which the formation of such phases was mainly attributed to the separation of chemically incompatible entities [4]. Continuous phases are less frequent for thermotropic mesogenic materials where the formation of one or more continuous networks is believed to be due to a mismatch between the volumes necessary to accommodate chemically incompatible molecular parts: alkyl chains and aromatic cores [5]. Typically, continuous phases exhibit cubic symmetry, which makes their properties isotropic, despite of their complexity. The most common cubic continuous phase is a double gyroid phase. This phase consists of two entangled continuous networks (a bi-continuous phase) of opposite chirality, related to each other by an inversion symmetry [6]. The gyroid structure is one of the most complex self-assembled continuous structures in nature [7]. The two networks are in fact two systems of channels, each made of linear units interconnected through flat three-fold junctions (nodes), the planes of adjacent nodes being twisted by ~ 70 degrees (Fig 1). The phase is achiral and belongs to the space group $Ia\bar{3}d$. What seems to be unique for the gyroid structure built from rod-like mesogenic molecules is a helical orientation of molecules along the channels [8-10]. The sense of molecular rotation is defined by the helical structure of channels - if molecular long axes are oriented perpendicular to the node-plane, then they have to twist between the nodes with the sense uniquely defined by the sense of rotation of adjacent junctions (Fig. 1). Another type of a cubic continuous phase, that turned out to be chiral [9], has been discovered in several materials [11-12], and based on the X-ray diffraction (XRD) studies, it was proposed to have a tri-continuous structure [13] or one continuous network that encloses micelles formed by the remnant molecules not included in the hexagonal network [14] (Fig. 2).

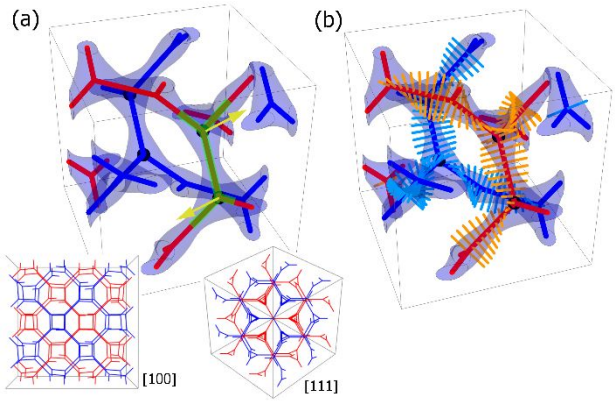

Figure 1. Structure of the $Ia\bar{3}d$ phase: (a) Structure of the $Ia\bar{3}d$ phase and a scheme of the repeating unit involving two neighboring nodes (marked in green), the junctions in adjacent nodes being twisted by ≈ 70 deg (yellow arrows are normal to the node planes). In the inset, the system of channels is viewed along the $[100]$ and $[111]$ directions, channels drown in red and blue are mirror inverted to each other. (b) Channels of the $Ia\bar{3}d$ phase decorated with rod-like molecules; molecules along each line connecting two nodes form short helices with the sense uniquely defined by the sense of rotation of the adjacent junctions.

[a] Department of Physics, Faculty of Natural Sciences and Mathematics, University of Maribor, Koroška 160, 2000 Maribor, Slovenia.
[b] Jozef Stefan Institute, Jamova 39, 1000 Ljubljana, Slovenia.
[c] Faculty of Chemistry, University of Warsaw, Żwirki i Wigury 101, 02-089 Warsaw, Poland.
[d] Advanced Light Source, Lawrence Berkeley National Laboratory, 1 Cyclotron Rd, Berkeley, CA 94720, USA.
[e] Department of Mathematics, University of Hamburg, Bundesstrasse 55, 20146 Hamburg, Germany
* corresponding authors: natasa.vaupotic@um.si, gorecka@chem.uw.edu.pl
Electronic Supplementary Information (ESI) available: modelling of XRD response and elastic energy. See DOI: 10.1039/x0xx00000x

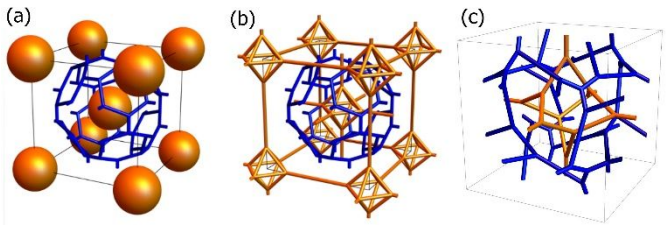

Figure 2. Current models of the chiral cubic phase: (a) Model with one continuous network and micelles and (b) tri-continuous model with the $Im\bar{3}m$ symmetry. In both cases the blue network is shown only within the unit cell, the micelle and the octagon in the center of the blue network also belong to the unit cell while the structures in the corner of the unit cell are shown in full, although belonging partially to the neighboring unit cells. c) Recently proposed tri-continuous model with the $I23$ symmetry. Only the inner and the middle grid are shown. The outer grid consists of the inner pattern transferred to all the corners.

The proposed continuous network, being characteristic for both models, is consistent with an increase of the crystallographic unit cell parameter from ~ 2 to ~ 3 molecular lengths, observed upon a transition from the double gyroid to the chiral cubic phase [15]. The structure with micelles is in line with the findings of the maximum entropy method [14] and density fluctuations study [16]. This cubic phase was, at first, assigned to have the $Im\bar{3}m$ symmetry, but due to its optical activity, it does not possess a center of inversion so its symmetry is lower. We shall call this phase the chiral cubic (CC) phase. A common characteristic of both models of the CC phase (Fig. 2) is a continuous network formed by a system of channels that meet in three-way junctions to form eight interconnected hexagons in the unit cell. This system of hexagons is assumed to be embedded on the Schwarz minimal surface [15,17]. The optical activity has been attributed to the formation of helices by a mechanism similar to the one in the $Ia\bar{3}d$ phase, where it results from a different orientation of molecules in the neighboring nodes [9]. By assuming the same sense of rotation of molecules along the sides of hexagon, two type of junctions are formed in the each hexagon, three with perfect and three with imperfect match in molecular orientation [9]. However, there is no specific reason why the helicity of each hexagon should be uniform; because the double gyroid phase is achiral, hexagons can be formed from equal amounts of left and right-handed segments. Indeed, by assuming that molecules are oriented in the direction "perpendicular" to each junction, where "perpendicular" means in the direction obtained by the sum of the unit vectors along the three channels forming the junction, careful inspection shows that there are three left and three right-handed helices within each hexagon, the structure thus being essentially achiral. In ref. [18] this problem is overcome by a continuous rotation of molecules on each micelle, which makes the micelles chiral. Such an arrangement would cause a strongly non-uniform density of micelles, which, to some extent can be observed also in the reconstruction of the electron density map from the XRD data, but the density inhomogeneity of micelles is very weak.

Just recently, a new structural model of the chiral cubic phase was proposed by the (co-)authors of the first tri-continuous structure [19]. The model still consists of three continuous grids but the connections in the inner and outer grid are chosen such that all the junctions are three-fold (Fig. 2). The obtained symmetry is $I23$, so the middle grid was structured such that it also has the $I23$ symmetry. All the grids can be of either the same or different chirality, based on a similar reasoning as in [9]. The structure is argued to give a very good agreement between the experimental measurements and model predictions. The reconstruction from experimental XRD intensities with phases of the peaks obtained from the model is indeed in good agreement with the model, but this is valid also for the previous models. The problem arises in a comparison of the model and experimental XRD intensities. Neither the first [20] nor the latest [19] tri-continuous model would give the (004) peak as the second highest in intensity. We also point out that such a model requires a significant rearrangement of molecules compared to the structure of the $Ia\bar{3}d$ phase from which the chiral phase evolves. This should be accompanied by a measurable enthalpy changes at the phase transition. However, for all the so far observed cases the enthalpy change is negligible.

In this paper we report on new experimental data from a new type of polycatenar materials exhibiting sequence of the chiral cubic and achiral double gyroid phases. Based on no observable enthalpy changes accompanying the phase transition between the CC and $Ia\bar{3}d$ phase we propose a new model of the CC phase that gives the elastic energy of the CC phase similar to the one of the double gyroid phase, it gives a good agreement with the XRD data (the highest peaks in the model are also the highest peaks observed in experiment), and we offer a new origin of chirality that overcomes the above mentioned problems of the existing models.

Results

Molecules of the studied materials (Fig. 3) have the same mesogenic core and they differ in the length of the terminal chain (R) at the biphenyl unit. On heating, the studied materials exhibit the CC phase at temperatures below the double gyroid phase (Table 1). On cooling, the double gyroid phase deforms into a metastable orthorhombic phase [21]. For the studied materials, the X-ray diffraction patterns were recorded as a function of temperature, which revealed a sequence of 3D-ordered phases (Fig. 4a). The DSC studies showed no or very small enthalpy changes accompanying these transitions (Fig. 4c), which seems like a general feature [11]. Upon melting the crystal, the consecutive phases in the heating scans are: $CC \rightarrow Ia\bar{3}d \rightarrow Col_h \rightarrow Iso$.

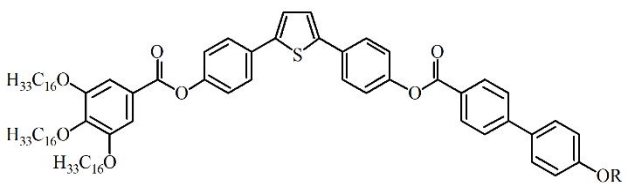

Figure 3. Studied materials: molecular structure of the studied materials.

Table 1. Phase sequences: Transition temperatures for the studied compounds (in °C) and associated enthalpy changes (given in brackets in Jg^{-1}) observed in heating scans for the studied homologues. The CC - $Ia\bar{3}d$ transition is not accompanied by a measurable thermal effect (the enthalpy change is below $0.005\ \mathrm{Jg}^{-1}$), the transition temperatures were obtained from the XRD studies.

R	Phase sequence
C_4H_9	Cr 106.5 (19.0) CC 175 $Ia\bar{3}d$ 181 Col_h 185.1 (1.1) Iso
C_5H_{11}	Cr 100.7 (32.3) Cr2 117.1 (1.0) CC 161 $Ia\bar{3}d$ 171 Col_h 180.7 (0.9) Iso
C_6H_{13}	Cr 108.8 (29.8) CC 176 $Ia\bar{3}d$ 179 Col_h 185.9 (1.4) Iso
C_8H_{17}	Cr 83.3 (23.2) Cr_2 96.5 (8.1) CC 160.5 (0.1) $Ia\bar{3}d$ 174.0 (0.02) Col_h 183.8 (1.1) Iso

In the hexagonal columnar phase (Col_h), the crystallographic unit cell parameter (column diameter) is consistent with a molecular length and in the gyroid and CC phases it corresponds to 2 and 3 molecular lengths, respectively. Both cubic phases have zero optical birefringence and the CC phase exhibits domains with a low optical activity, ~ 0.5 degree/μm (Fig. 4d).

Discussion

The intensities of the experimentally obtained diffraction peaks in the CC phase are given in Table 2. The highest intensity peaks are the ones with the Miller indices (hkl) equal to (123) and (004), which is characteristic for all the so far studied CC phases. The electron density $\rho(\vec{r})$ map is reconstructed from the amplitudes of the form factors ($|F_{hkl}|$) and their phases (ϕ_{hkl}) as

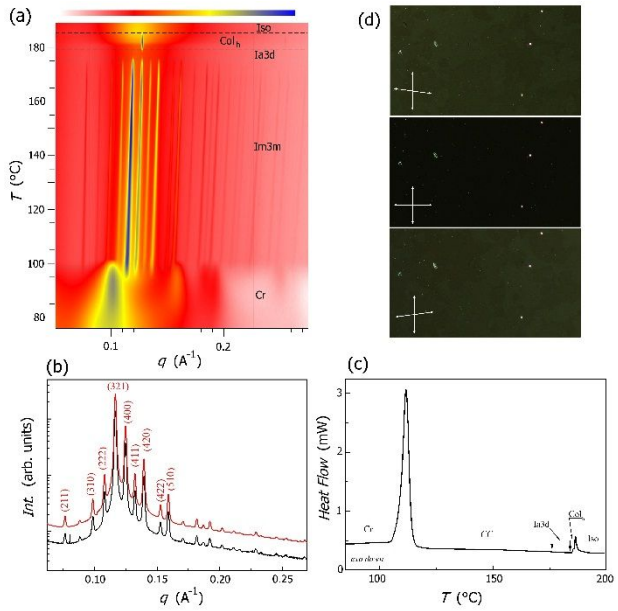

Figure 4. Experimental data for the compound with R=C_6H_{13} (a) Temperature evolution of X-ray diffraction signals observed on heating, (b) XRD pattern taken in *CC* phase; black and red lines show experimental and simulated patterns, respectively. (c) DSC thermogram taken on a heating scan; arrows mark temperatures of a phase transition detected by the XRD studies. (d) Optically isotropic texture of the *CC* phase; the domains showing optical activity are visible under slightly de-crossed polarizers.

$$\rho(\vec{r}) = \sum_{h,k,l} |F_{hkl}| \cos\left(\vec{q}\cdot\vec{r} + \phi_{hkl}\right),$$

where $\vec{q}$ is a scattering vector. In a general case, structure factors are complex numbers. From a standard X-ray experiments only information related to the amplitude of the structure factors is available (a square root of the signal intensity), while the information about the structure factor phase is lost. For structures with a center of inversion the phase ϕ_{hkl} can be only 0 or π; however, for a structure without the inversion symmetry, the peak (123) can have any phase between 0 and π and if the symmetry is low enough then permutations of the Miller indices do not give equivalent peaks [19]. Because no enthalpy change is observed upon the phase transition from the double gyroid to the chiral cubic phase, we focus on the structural models with the middle grid made of hexagons, as their side can be made equal to the length of the connections between the neighboring nods in the double gyroid phase. All the possibilities of combination of phases of the (123) peak for structures with the symmetry $I432$ or $I\bar{4}3m$ have already been studied in detail and the corresponding density maps are shown in [20]. It is shown that the electron density maps reconstructed with a general phase of the (123) peak are closely related to the electron density maps obtained for the $Im\bar{3}m$ symmetry structure. However, large deviation of ϕ_{123} from 0 and π values introduce degrees of distortion, which are not physically plausible. We thus assumed that the phase ϕ_{123} is close to either 0 or π. For the reconstruction of the electron density distribution in the CC phase (Fig. 5) the four highest intensity signals were taken ((123), (004), (024) and (222)), the first two already giving the major properties of the structure. The structure factor of the peak (123) was taken to be negative ($\phi_{123} = \pi$) and the structure factors of peaks (024) and (222) positive. Regardless of the sign of the (004) signal, there are micellar objects in the corners and in the middle of the unit cell and a continuous network of channels composed of hexagonal units between them.

Table 2. X-ray studies of the CC phase: Experimental intensities ($I_{hkl}^{(exp)}$) of the peaks with Miller indices (h,k,l), multiplicity of the peaks (M) and intensities (I_{M2}) obtained from model 2. Parameter values: coordinates of the generating point $(0.151,0.151,0.425)a_{CC}$; $r_m = 0.22a_{CC}$, $\Delta r_m = 0.05a_{CC}$, $r_c = 0.075a_{CC}$, $\rho_{cc}/\rho_m = 0.3$.

(h,k,l)	M	$I_{hkl}^{(exp)}$	I_{M2}
011	12		0.03
002	6		0.03
112	24	0.002	0.06
022	12	0.001	0.02
013	24	0.007	0.06
222	8	0.057	0.001
123	48	1	1
004	6	0.26	0.25
114	24	0.03	0.004
033	12		
024	24	0.06	0.16
233	24		0.04
224	24	0.005	0.08

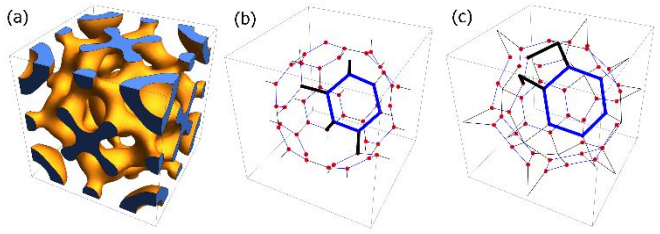

Figure 5. Structure of the CC phase: (a) The electron density map reconstructed from the experimental data by assuming the phases of the (123) and (004) being both π. The scheme of the middle network considered in: (b) model 1 and (c) model 2. The rods forming the hexagons are colored blue and the connecting rods are plotted in black. In model 1, we match the lengths (l) of the rods in hexagons with the rods connecting the hexagons as well as the angles among the three rods meeting in a junction (red points). In model 2, apexes of the hexagons are connected to either centers of the edge of a cube or the center of its face.

By considering the size of the network segments and micelles, it was estimated that approximately 60% of molecules form the hexagon network and the rest form the micelles. If the structure factor of the peak (004) is negative, single spherical or slightly distorted spherical micelles are present. The distortion was previously considered to be due to a chiral arrangement of mesogenic cores on the periphery of a micelle [16]. For a positive sign of the (004) peak one obtains groups of smaller micelles, which were considered as an indication of an octahedral arrangement of linear segments [13, 20].

A common characteristic of both electron density maps (for the negative and positive sign of the structure factor of the peak (004)) is a network that is built of linear segments connected by 3-fold junctions to form hexagons. The length and diameter of the segments are similar to those forming helical channels of the $Ia\bar{3}d$ phase. By comparing the maps obtained with either a negative or positive phase of the (004) signals (at a high density cut-off), it can be seen that the one with a negative sign of the (004) signal provides a more uniform density along the hexagon network (Supplementary Figure 1). In what follows we shall consider only the structure with one continuous network and micelles (the one being in line with the findings of the maximum entropy method [14] and density fluctuation studies [16]), from which it follows that (*i*) the structure is stabilized if the phases of the (123) and (004) peaks are equal and (*ii*) the volume occupied by higher density regions is less than half of a unit cell if both phases are π. To have a more detailed insight in the structure of the CC phase, we constructed a model by assuming that the continuous network structure itself is centrosymmetric (thus having the $Im\bar{3}m$ symmetry), while the arrangement of molecules on the network is such as to lead to some remnant optical activity. Such arrangement, however, should not affect significantly the electron density distribution and, as a result, the non-resonant XRD response. Thus, a model of the continuous network was constructed, in which the positions of the nodes were generated from an arbitrary point inside a unit cell by its crystallographic equivalents for the $Im\bar{3}m$ symmetry and the nodes were connected by linear segments (rods). By a suitable choice of the generating point, one can match the lengths of the rods connecting the nodes as well as the angles between the rods. There are two possibilities to find the coordinates of the nodes and connections that fit the $Im\bar{3}m$ symmetry: (1) the edges of the hexagons are of the same length as the distances between the nearest apexes of the neighboring hexagons and (2) the edges of the hexagons are of the same length as the distances from the hexagon apexes to the centers of the unit cell faces or edges (Fig. 5).

In the first case, apexes of the neighboring hexagons are directly connected through linear segments, while in the second case, the connections are through additional nodes, which results in the whole network being built of interconnected hexagons. For case (1) there are two solutions. We discard the one in which the angles between linear segments are 90 deg. The other generating point has coordinates $(0.181, 0.181, 0.407)a_{CC}$, a_{CC} being the unit cell length in the CC phase. In this model (Model 1) the length of the hexagon edges is $0.181a_{CC}$, very close to the value $0.183\ a_{CC}$ used in [13], the angle between the rods meeting in each hexagon apex is 118.6 deg. For case (2), there is only one solution (Model 2) with the generating point at $(0.151,0.151,0.425)a_{CC}$; the length of the hexagon edges is $0.226a_{CC}$ and the angle between the linear segments is 118.5 deg. Both models give almost planar 3-fold junctions of channels (in the $Ia\bar{3}d$ phase the junctions are exactly planar); however, Model 2 gives the length (l) of the channels within the hexagons almost equal to the length of the channels in the $Ia\bar{3}d$ phase ($l = 0.34\ a_{DG}$ in the CC phase and $l = 0.35\ a_{DG}$ in the $Ia\bar{3}d$ phase, where a_{DG} is the unit cell parameter of the double gyroid phase), while in Model 1 the length of channels within the hexagons is $l = 0.27\ a_{DG}$, much lower than in the $Ia\bar{3}d$ phase.

The form factor of the unit cell is calculated as follows (details are given in the Supplementary Information). Micelles of a medium radius r_m and thickness Δr_m are placed in the corners of the unit cell and in its center. The connections between the nodes are modelled by cylinders, their length being given by the length of the connecting rods. The densities of the micelles (ρ_m) and the cylinders of the middle network (ρ_c) are assumed to be equal, while the density of the cylinders connecting the hexagon apexes with the additional junctions on the edges or faces of the unit cell is lower (ρ_{cc}), as concluded from the experimentally obtained electron density maps (Supplementary Figure 1). There are thus three fitting parameters (r_m, Δr_m, r_c) for Model 1 and four fitting parameters (r_m, Δr_m, r_c, ρ_{cc}) for Model 2. The fitting parameters are adjusted in order to yield the calculated relative diffraction signal intensities matching those obtained experimentally; results are collected in Table 2, but only for model 2. Model 1 does not give any, even remotely, satisfactory match, as it is impossible to obtain a proper intensity ratio even between the two highest peaks (123) and (004). The same problem was encountered for the structure with octagons in the outer and inner networks [13]; no satisfactory match has been found [19], as the model intensities of the (013) and (024) peaks were calculated to be (much) higher than the intensity of the (004) peak. The fitting parameters of Model 2 are strongly restricted by the lowest-angle peaks, resulting in a narrow range of model parameters matching the observed intensities. From Table 2 we see that Model 2 gives a good match to the experimentally observed intensities. Its only flaw seems to be

that it predicts a too low intensity value for the (222) peak. Experimentally, the (222) peak is one of the four highest peaks (see Table 2), but still, much lower than the peaks (123) and (004).

Interestingly, the proposed model shows that the minimal surface on which the hexagon network is embedded is closer to the Neovius surface (Fig. 6a) rather than the previously suggested Schwarz primitive one [15,17] (Fig. 6b). In fact, the best fit is given by a degeneration of the Neovius surface known as the WP-surface (Fig. 6c). The WP surface is also in line with the prediction of micellar structures in the corners and center of the unit cell. The micelles correspond to the translation of each point on the minimal surface in the direction perpendicular to it.

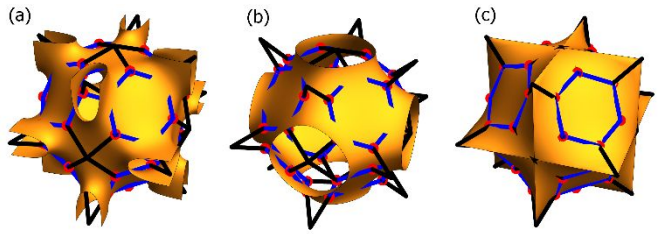

Figure 6. The hexagon network of the CC at the minimal surface: the hexagon network of Model 2 placed on the (a) Neovius surface, (b) Schwarz primitive surface and (c) WP surface.

Due to a negligible enthalpy change at the phase transition, the stabilization of different phases critically depends on the elastic energy of the assembly. We model the latter by choosing a surface of a constant critical density (iso-electron-density surface), such that the volume enclosed by it corresponds to the volume occupied by aromatic cores. We assume that other contributions to the total energy of the phase remain the same at phase transition (which is supported by the enthalpy measurements), thus elastic energy plays a deciding role in the mechanism of the phase transition. Such an approach does not consider the energy due to a possible mismatch (defect) in the nodes. The number of three-fold nodes in the double gyroid unit cell is 16, which, rescaled to the unit cell of the chiral phase, gives 56 nodes. In our model, there are 48 three-fold nodes on the continuous grid, 3 eight-fold on the faces and 3 eight-fold nodes on the edges. The energy of the three-fold nodes is assumed to be the same in the chiral and double gyroid phase. The energy of the eight-fold nodes is expected to be higher, but the density is lower there. Therefore we assume that the energy related to the nodes is comparable in both phases and we neglect this contribution. The Helfrich energy (μ_C) of the iso-electron-density surface is defined as

$$\mu_C = \int_S \left(\frac{1}{2}\kappa_H (H - H_0)^2 + \kappa_G K \right) dS$$

where H and K are the mean and the Gaussian curvature, respectively, and κ_H and κ_G are the corresponding moduli. In a series of experiments [22-25], it was observed that $\kappa_G \simeq -\kappa_H$, but as shown in the Supplementary Figure 2, the ratio between the magnitudes does not play a role in our computations. By H_0 we denote the natural curvature of the assemblies, which is zero for the studied system. The Gauss-Bonnet theorem dictates $\int_S K dS = 4\pi(1-g)$, where g is the genus of the surface, thus the Gaussian curvature modulus plays an important role only when phase transitions involving the change of topology are considered. It was found that the iso-electron-density surface generated with both structure factors (321) and (004) taken negative yields a much better match in the elastic energies of the CC and $Ia\bar{3}d$ phases, than the surface obtained by taking structure factors of opposite signs. The mean and Gaussian energies, together with the total Helfrich energy are collected in Supplementary Table 4. The ratio between the Helfrich energy of the structure with both the phases being π and the structure with the phase of (004) peak being 0 is approximately 0.71 if the iso-electron-density surface is chosen such that it encloses $1/3$ of the unit cell volume. The ratio varies only by few percent if higher or lower density cut-offs are chosen (see Supplementary Table 4). The ratio between the energy of the CC phase reconstructed with both phases being π and energy of an equal volume of the $Ia\bar{3}d$ phase is approximately 1.4 while it is approximately 2.1 if the phase of the (004) peak is 0. For the recently proposed model [19], as expected, the ratio (being 2.9) is even higher due to a high number of junctions.

Finally, we discuss the origin of optical activity. As already mentioned, the optical activity has, so far, been attributed to two different mechanisms: (*i*) chiral structure of the channels forming the networks in the tri-continuous model due to the helical variation of the long molecular axis along the channel between the neighboring nodes, with the chirality of the middle network being opposite to the chirality of the inner and outer networks [9] and (*ii*) a continuous rotation of molecules on micelles, which makes the micelles chiral [18]. In the first case, it is assumed that all the segments of the middle network have the same sense of helical rotation. Because the enthalpy change at the phase transition between the double gyroid and chiral cubic phase in very small, we conclude that the rearrangement of molecular position accompanying the transition is as small as possible. Because the left- and right-handed networks are neighboring in the double gyroid, it can be expected, that one hexagon is formed by the same amount of the right- and left-handed sides. If one draws lines in the direction either perpendicular to the nodes formed by three channels or only in the direction perpendicular to the two channels from the hexagon sides, it becomes evident that there is an equal amount of the right and left rotations when going around the hexagon.

Therefore we propose an alternative possibility: the symmetry breaking is caused by an alternating up-down inclination of molecules in the middle of the neighboring segments of each hexagon, which has an armchair geometry (Fig. 7). Such placing of molecules on the hexagon sides ensures a better space filling of alkyl chains inside the hexagon. Also, it is quite straightforward to see, that better packing conditions are obtained if the connected hexagons are of the same chirality (compare Figs 7a and 7b). We thus suggest, that the chirality from an individual hexagon propagates to the neighboring

hexagons and as a result large domains of the right and left-handed hexagonal network are formed.

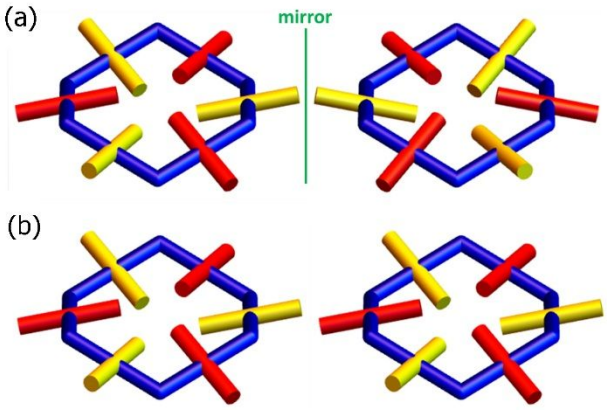

Figure 7. Origin of optical activity: The arrangement of molecules between the nodes of non-flat hexagons with an *armchair* conformation ensures a broken chiral symmetry of the structure. a) Two chiral conformations of the hexagon, one being the mirror image of the other. b) Two hexagons of the same chirality. Because the molecules in the nearest channels from different hexagons are tilted in the same direction this gives more space for aliphatic tails.

Conclusions

We studied the chiral cubic phase formed by new polycatenar materials. A good agreement among the experimental results and theoretical modelling is obtained only in the case of a structure with one continuous network into which micelles are embedded. Based on a negligibly small enthalpy change at the phase transition between the double gyroid and chiral cubic phase we propose that the continuous network is made of hexagons, the sides of which are equal to the distance between the neighboring junctions in the double gyroid phase. The hexagons are placed on the WP (deformed Neovius) and not on the Schwarz minimal surface, as considered previously. Such a structure, together with the additional channels connecting the hexagon edges to the centers of the unit cell faces and edges gives a good agreement of the model and experimental XRD signal intensities, which could not be achieved when hexagons with smaller sides were chosen [20] nor in the case of structure with the $I23$ symmetry [19]. We estimated the elastic energy of the proposed structure and showed that it is comparable to the energy of the double gyroid phase. Finally, we proposed that the optical activity is caused by an alternating up-down inclination of molecules in the middle of the neighboring segments of the hexagon that has an armchair geometry. With such an arrangement, more space is achieved for tails both within one hexagon as well as between the neighboring hexagons in the continuous network. The ultimate knowledge on the molecular arrangement in the chiral cubic phase can probably be given by the resonant soft x-ray scattering which only recently proved to be a proper tool to unmask the molecular structure in the double gyroid phases [26].

Methods

The initial X-ray diffraction studies for all materials were performed with the Bruker Nanostar system (CuKα beam formed by cross-coupled Goebel mirrors and three-pinhole collimator, Vantec 2000 area detector). Samples were prepared as droplets on a heated surface. For chosen materials, additional X-ray measurements were carried out on the SAXS beam line (7.3.3) at the Advanced Light Source, Lawrence Berkeley National Laboratory at the wavelength 0.12398 nm. Samples were placed on a heating plate as droplets. The scattering intensity was recorded using the Pilatus 2M detector. Optical studies were performed by using the Zeiss Axio Imager A2m polarizing microscope equipped with a Linkam heating stage. Samples were observed in glass cells of various thicknesses: from 1.8 to 10 μm. Calorimetric studies were performed with a TA DSC Q200 calorimeter, samples of mass from 1 to 3 mg were sealed in aluminum pans and kept in nitrogen atmosphere during measurement, both heating and cooling scans were performed with a rate of $5-10$ K/min.

Conflicts of interest

There are no conflicts to declare.

Acknowledgements

M.S., D.P., and N.V. acknowledge the support of the National Science Centre (Poland) under the grant no. 2016/22/A/ST5/00319. E.G. acknowledges the funding from the Foundation for Polish Science through the Sabbatical Fellowships Program. N.V. acknowledges the support of the Slovenian Research Agency (ARRS), through the research core funding no. P1-0055. The work of M.V. is supported by the DFG Emmy-Noether grant number AL 1407/2-1. The beamline 11.0.1.2 at the Advanced Light Source at the Lawrence Berkeley National Laboratory is supported by the director of the Office of Science, Office of Basic Energy Sciences, of the U.S. Department of Energy under Contract No. DE-AC02-05CH11231.

Notes and references

1 M. Pelanconi, A. Ortona, *Materials,* 2019, **12**, 4134.
2 E. J. W. Crossland, M. Kamperman, M. Nedelcu, C. Ducati, U. Wiesner, D.-M. Smilgies, G. E. S. Toombes, M. A. Hillmyer, S. Ludwigs, U. Steiner, H. J. Snaith, *Nano Lett.* 2009, **9**, 2807-2812.
3 J. A. Dolan, B. D. Wilts, S. Vignolini, J. J. Baumberg, U. Steiner, T. D. Wilkinson, *Adv. Optical Mater*., 2015, **3**, 12–32.
4 P. J. Flory, *Principles of Polymer Chemistry*; Cornell University Press: Ithaca, NY, USA, 1953.
5 C. Tschierske, *J. Mater. Chem*., 2001, **11**, 2647-2671.
6 D. Guillon, A. Skoulios, *Europhys. Lett.,* 1987, **3**, 79-85.
7 G. E. Schröder-Turk , S. Wickham , H. Averdunk , F. Brink , J. D. Fitz Gerald , L. Poladian , M. C.J. Large , S. T. Hyde , *J. Struct. Biol.,* 2011 , **174** , 290-295.
8 Y. Nakazawa, Y. Yamamura, S. Kutsumizu, and K. Saito, *J. Phys. Soc. Jap.,* 2012, **81**, 094601.
9 C. Dressel, F. Liu, M. Prehm, X. Zeng, G. Ungar, C. Tschierske, *Angew. Chem. Int. Ed.,* 2014, **53**, 13115-13120.
10 C. Tschierske, G. Ungar, *ChemPhysChem*, 2016, **17**, 9–26.

11 S. Kutsumizu, T. Ichikawa, S. Nojima, S. Yano, *Chem. Commun*., 1999, 1181-1182.
12 M. Imperor-Clerc, P. Sotta, M. Veber, *Liq. Cryst.,* 2000, **27**, 1001- 1009.
13 X. Zeng, G. Ungar, M. Impéror-Clerc, *Nat. Mater.,* 2005, **4**, 562–567.
14 K. Ozawa, Y. Yamamura, S. Yasuzuka, H. Mori, S. Kutsumizu, K. Saito, *J. Phys. Chem. B.,* 2008, **112**, 12179-81.
15 S. Kutsumizu , K. Morita , S. Yano, S. Nojima, *Liq. Cryst.,* 2002, **29**, 1459- 1468.
16 K. Saito, Y. Yamamura, S. Kutsumizu, *J. Phys. Soc. Jap.,* 2008, **77**, 093601.
17 K. Saito, M. Sorai, *Chem. Phys. Lett.,* 2002, **366**, 56-61.
18 K. Saito, Y. Yamamura, Y. Miwa, S. Kutzumizu, *Phys.Chem.Chem.Phys.,* 2016, **18**, 3280-3284.
19 X. Zeng and G. Ungar, *J. Mater. Chem. C*, 2020, **8**, 5389-5398.
20 X. Zeng, L. Cseh, G. H. Mehl, and G. Ungar, *J. Mater. Chem.* 2008, **18**, 2953-2961.
21 J. Matraszek, D. Pociecha, N. Vaupotič, M. Salamończyk, M. Vogrin, E. Gorecka, *Soft Matter,* 2020, **16**, 3882-3885.
22 R. H. Templer, J. M. Seddon, N. A. Warrender, A. Syrykh, Z. Huang, R. Winter, J. Erbes, *J. Phys. Chem. B,* 1998, **102**, 7251-7261.
23 R. H. Templer, B. J. Khoo and J. M. Seddon, *Langmuir*, 1998, **14**, 7427-7434.
24 H. Vacklin, B. J. Khoo, K. H. Madan, J. M. Seddon, R. H. Templer, *Langmuir,* 2000, **16**, 4741-4748.
25 J. Zimmerberg, M. M. Kozlov, *Nat. Rev. Mol. Cell. Biol.,* 2006, **7**, 9-19.
26 Y. Cao, M. Alaasar, A. Nallapaneni, M. Salamo ń czyk, P. Marinko, E. Gorecka, C. Tschierske, F. Liu, N. Vaupotič, C. Zhu, *submitted*